Open access • Journal Article • DOI:10.1007/S00466-006-0072-7

Identification of Chaos Representations of Elastic Properties of Random Media Using Experimental Vibration Tests — Source link

Christophe Desceliers, Christian Soize, Roger Ghanem

Institutions: University of Marne-la-Vallée, University of Southern California

Published on: 22 Feb 2007 - Computational Mechanics (Springer-Verlag)

Topics: Polynomial chaos, Random field, Random function, Random element and Random compact set

Identification of chaos representations of elastic properties of random media using experimental vibration tests

Christophe Desceliers, Christian Soize, R. Ghanem

C. Desceliers · C. Soize · R. Ghanem

Identification of chaos representations of elastic properties of random media using experimental vibration tests

Received: date / Accepted: date

Abstract This paper deals with the experimental identification of the probabilistic representation of a random field modelling the Young modulus of a non homogeneous isotropic elastic medium by experimental vibration tests. Experimental data are constituted of frequency response functions on a given frequency band and for a set of observed degrees of freedom on the boundary of specimens. The random field representation is based on the polynomial chaos decomposition. The coefficients of the polynomial chaos are identified setting an inverse problem and then in solving an optimization problem related to the maximum likelihood principle.

Keywords Identification · Elastic random medium · Polynomial chaos

1 Introduction

Analysis and modelling of random media have received considerable attention over the past decade by scientists and engineers (see, for instance, [5; 6; 8; 9; 12; 14; 17]). A fundamental question concerns the experimental identification of the probabilistic model of the elastic properties of such media solving a stochastic inverse problem. Only a few works have been published in this field (see for instance [1; 2; 11; 16]). Such a problem has recently be adressed in [3] for the identification of the chaos representation of the Young modulus of an elastic random media using experimental static tests. The method in [3] consists (1) in using a polynomial chaos representation of the random field (see for instance [4; 13; 15]) to be identified,(2) in constructing an estimation of the coefficients of the chaos representation by using the maximum likelihood method. In this work, the experimental tests are static which generally require a lot of experimental measurements for a very heterogeneous random medium. In this paper, an extension of this method is presented in the context of experimental vibration tests. The objective is (1) to use the measured frequency response functions which allow the quality of the construction to be increased with respect to the case for which static measurements are available and (2) to have a method based on the use of experimental vibration tests which are often easier to perform than static tests.

The proposed method is presented through a complex example related to the experimental identification of the random field modelling the Young modulus of a linear isotropic heterogeneous random medium by vibration tests. The data used for the identification are the frequency response functions related to the displacement field on the boundary of a set of specimen. The same external load are used for each specimen of the experimental database. The spectrum of the external loads is constant on the frequency band of analysis. The method consists in (1) discretizing the elastodynamic problem by using the finite element method for each specimen, (2) estimating the coefficients of the finite element representation of the random field to identify by setting an optimization problem for each specimen of the experimental database, (3) constructing the polynomial Chaos representation of the random field and (5) estimating the coefficients of the polynomial Chaos representation by using the maximum likeligood method. Then, the probabilistic model of the random Young modulus field will be completely defined.

C. Desceliers
Université Marne-La-Vallée, Paris, France
Tel.: +33-1-60957779
Fax: +33-1-60957799
E-mail: christophe.desceliers@univ-mlv.fr

C. Soize
Université Marne-La-Vallée, Paris, France

R. Ghanem
University of Southern California, California, USA

2 Construction of an "experimental database"

The specimen is constituted of a non-homogeneous isotropic linear elastic medium occupying a three-dimen-

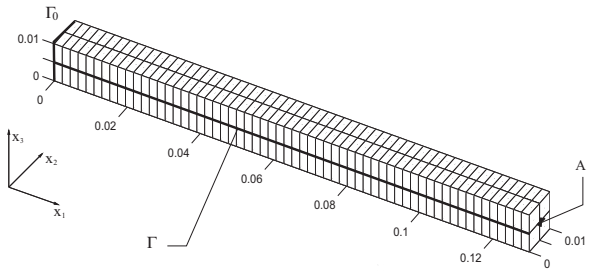

Fig. 1 Definition of the specimen

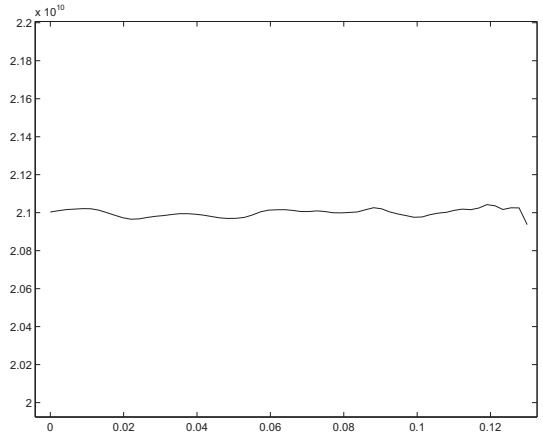

Fig. 2 Graph of the function $\mathbf{x} \mapsto E\{Y(\mathbf{x})\}$ where $\mathbf{x} = (x_1, x_2, x_3)$ with $x_2 = x_3 = 0$. Horizontal axis: x_1. Vertical axis: $E\{Y(\mathbf{x})\}$.

sional bounded domain $\mathcal{D}$ with boundary $\partial\mathcal{D}$ given in a Cartesian system $Ox_1x_2x_3$. The geometry of domain $\mathcal{D}$ is a slender rectangular box shown in Fig. 1 whose dimensions along x_1, x_2 and x_3 are $L_1 = 1.3 \times 10^{-1}m$, $L_2 = 2 \times 10^{-2}m$ and $L_3 = 2 \times 10^{-2}m$. This elastic medium is random. It is assumed that the Young modulus is random while the Poisson coefficient $\nu = 0.3$ and the mass density $\rho = 2.7 \times 10^3\, Kg/m^3$ are deterministic. The random Young modulus field is modeled by a positive-valued second-order random field $Y(\mathbf{x})$ defined in Appendix A. and independent of x_2 and x_3. Figure 2 shows the mean value $\mathbf{x} \mapsto E\{Y(\mathbf{x})\}$ where $E\{\}$ denotes the mathematical expectation. Figure 3 shows the graph of the autocorrelation function $(\mathbf{x}, \mathbf{x}') \mapsto E\{Y(\mathbf{x})Y(\mathbf{x}')\}$. It can be shown that the correlation length of the random Young modulus is much smaller than the length L_1 of the specimen.

The specimen is fixed on the part Γ_0 of boundary $\partial\mathcal{D}$ for which the displacement field is zero. The specimen is subjected to an external point force denoted as $\mathbf{b}(t)$ and applied to the node A along x_1-axis (see Fig. 1). The Fourier transform $\widehat{\mathbf{b}}$ of $\mathbf{b}$ is the constant vector $(1, 0, 0)$ in the frequency band $\mathbb{B} = [0, 50]$ kHz. Let $m = 100$

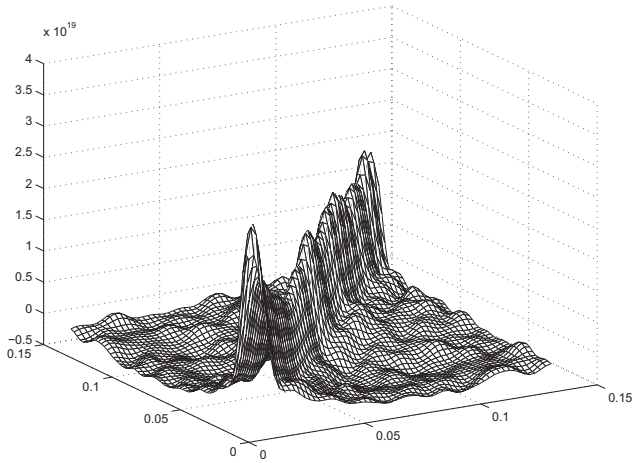

Fig. 3 Graph of the function $(\mathbf{x}, \mathbf{x}') \mapsto E\{Y(\mathbf{x})Y(\mathbf{x}')\}$ where $\mathbf{x} = (x_1, x_2, x_3)$ and $\mathbf{x}' = (x_1', x_2', x_3')$ with $x_2 = x_3 = 0$ and $x_2' = x_3' = 0$. Horizontal axis: x_1 and x_1'. Vertical axis: $E\{Y(\mathbf{x})Y(\mathbf{x}')\}$.

be the total number of specimen used for constructing the experimental database. For each specimen, the experimental measurements consist in $N_b = 60$ frequency response functions related to the displacement along x_1-axis of the nodes belonging to the part Γ of boundary $\mathcal{D}$ (see Fig. 1) and where ω is running through the frequency band of analysis. Let $\mathbf{u}_\Gamma^1(\omega), \ldots, \mathbf{u}_\Gamma^m(\omega)$ be the m vectors belonging to $\mathbb{R}^{N_b}$ whose elements correspond to the frequency response functions of each specimen and constituting the experimental database. In this paper, the experimental database is constructed by numerical simulations of the direct problem (see Annexe B).

3 Identification of the realizations of the random Young modulus by solving an inverse problem for each specimen of the database

The finite element mesh of the structure is shown in Fig. 1 and consists of 8-node isoparametric 3D solid finite elements. There are $N_d = 1620$ degrees of freedom. The finite element approximation of the Young modulus is modeled by the random field $\widetilde{Y}$ indexed by $\mathcal{D}$ and written as

$$\widetilde{Y}(\mathbf{x}) = \sum_{k=1}^{N} R_k h_k(x_1) \qquad (1)$$

in which $h_1(x_1), \ldots, h_N(x_1)$ are the usual linear interpolation functions related to the finite element mesh of domain $\mathcal{D}$, where $N = 60$ is the degree of this approximation and where $R_1, \ldots R_N$ are random coefficients. We introduce the $\mathbb{R}^N$-valued random variable $\mathbf{R}$ such that $\mathbf{R} = (R_1, \ldots, R_N)$. Eq (1) can then be rewritten as

$$\widetilde{Y}(\mathbf{x}) = \mathbf{h}(x_1)^T\, \mathbf{R} \qquad (2)$$

in which $\mathbf{h}(x_1) = (h_1(x_1), \ldots, h_N(x_1))$ and where exponent ^{T} means the transpose of a matrix. Let $[K(\mathbf{R})]$ be the random stiffness matrix with values in the set of all the positive-definite symmetric $(N_d \times N_d)$ real matrices constructed by using the finite element approximation $\widetilde{Y}(\mathbf{x})$ of the Young modulus. Let $[M]$ and $[D]$ be the mass and the damping matrices such that $[D] = a\,[M]$ with $a = 10^4\, s^{-1}$. Matrices $[M]$ and $[D]$ are deterministic positive-definite symmetric $(N_d \times N_d)$ real matrices. The $\mathbb{R}^{N_d}$-valued random-frequency-response function $\omega \mapsto \mathbf{U}(\omega)$ related to the nodal displacements is such that

$$[A(\omega;\mathbf{R})]\mathbf{U}(\omega) = \mathbf{f}(\omega) \quad ,$$

in which

$$[A(\omega;\mathbf{R})] = \; -\omega^2\,[M] + i\,\omega\,[D] + [K(\mathbf{R})]$$

where $\mathbf{f}(\omega)$ is the $\mathbb{R}^{\mathbb{N}_d}$-vector of the external forces. Let $\omega \mapsto \mathbf{U}_\Gamma(\omega)$ be the $\mathbb{R}^{N_b}$-valued random-frequency-response function related to the nodal displacements along x_1-axis of nodes belonging on Γ. Let $\mathbb{P}$ be the linear mapping from $\mathbb{R}^{\mathbb{N}_d}$ into $\mathbb{R}^{\mathbb{N}_b}$ such that, for all ω belonging to the frequency band $\mathbb{B}$,

$$\mathbf{U}_\Gamma(\omega) = \mathbb{P}(\mathbf{U}(\omega)) \quad . \tag{3}$$

Realizations $\mathbf{R}(\theta_1), \ldots, \mathbf{R}(\theta_m)$ of random vector R are constructed by solving the following nonlinear optimization problems

$$\min_{\mathbf{R}(\theta_j)} \ell_{dyn}((\theta_j), \mathbf{u}^j_\Gamma) \quad , \quad \forall j = 1, \ldots, m \tag{4}$$

in which

$$\ell_{dyn}(\mathbf{R}(\theta_j), \mathbf{u}^j_\Gamma) = \sum_{k=1}^{N_{band}} \int_{B_k} \left\| \mathbb{P}\left([\widetilde{A}(\omega;\mathbf{R}(\theta_j))]^{-1}\mathbf{f}(\omega) \right) - \mathbf{u}^j_\Gamma(\omega) \right\|^2 d\omega \,. \tag{5}$$

in which $\|\cdot\|$ is the Euclidean norm. In the right-hand side of Eq. (5) , $B_k = [\omega_{\min,k}, \omega_{\max,k}]$ with $\omega_{\min,k} = \omega_k - B_{eq,k}/2$ and $\omega_{\max,k} = \omega_k + B_{eq,k}/2$ in which $B_{eq,k} = \pi\, a \sqrt{1 - (a/2\omega_k)^2}$ and where $N_{band} = 5$ is the number of bands considered for the identification. It should be noted that the optimization problem introduced in [3] in order to solve the inverse problem to construct the realizations $\mathbf{R}(\theta_1), \ldots, \mathbf{R}(\theta_m)$ of random vector $\mathbf{R}$ is based on an elastostatic problem. In this case, the experimental database is constituted of static measurements related to the displacement field on the boundary of each specimen and the optimization problem is defined as

$$\min_{\mathbf{R}(\theta_j)} \ell_{stat}(\mathbf{R}(\theta_j), \mathbf{u}^j_\Gamma) \quad , \quad \forall j = 1, \ldots, m \tag{6}$$

in which

$$\ell_{stat}(\mathbf{R}(\theta_j), \mathbf{u}^j_\Gamma) = \left\| \mathbb{P}\left([\widetilde{A}(0;\mathbf{R}(\theta_j))]^{-1}\mathbf{f}(0) \right) - \mathbf{u}^j_\Gamma(0) \right\|^2 \quad .$$

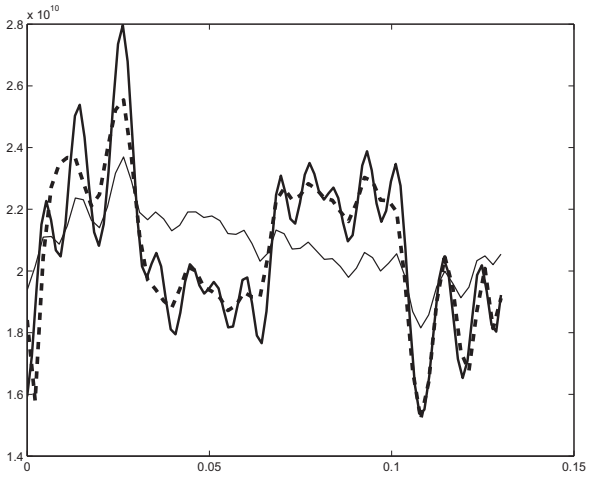

Fig. 4 Graph of a realization $x_1 \mapsto Y(\mathbf{x};\theta)$ of the Young modulus of the experimental database (thick solid line) and graph of a realization $x_1 \mapsto \widetilde{Y}(\mathbf{x},\theta)$ with $x_2 = x_3 = 0$ constructed by solving the "dynamic inverse problem" (dash line) with $N_{band} = 5$ and the "static inverse problem" (thin solid line). Horizontal axis: x_1. Vertical axis: $Y(\mathbf{x};\theta_1)$ and $\widetilde{Y}(\mathbf{x},\theta)$

The optimization problems defined by Eqs. (4) and (6) are solved by using a least-squares estimation of nonlinear parameters (see [7]). Realizations $\mathbf{x} \mapsto \widetilde{Y}^1(\mathbf{x},\theta_1), \ldots, \mathbf{x} \mapsto \widetilde{Y}^1(\mathbf{x},\theta_m)$ are constructed by using Eq. (2) . We then have

$$\widetilde{Y}^1(\mathbf{x},\theta_j) = \mathbf{h}(x_1)^T\,\mathbf{R}(\theta_j) \quad , \quad \forall j = 1, \ldots, m.$$

Figure 4 shows the graph of one realization $x_1 \mapsto \widetilde{Y}(\mathbf{x},\theta)$ with $x_2 = x_3 = 0$ constructed by solving Eq. (4) ("dynamic inverse problem") and Eq. (6) ("static inverse problem"). It can be seen that the dynamical inverse problem gives more accurate results than the static inverse problem. This can be explained by considering solving the dynamic inverse problem is equivalent to solve a static inverse problem for each value of ω belonging to the frequency band $\mathbb{B}$. The amount of available information used by the dynamic inverse problem is then much greater than the amount of available information used by the static inverse problem.

4 Statistical reduction

In order to identified the probabilistic model of the random field $\widehat{Y}$, the probabilistic model of the random vector $\mathbf{R}$ has to be constructed by setting a stochastic inverse problem using realizations $\mathbf{R}(\theta_1), \ldots, \mathbf{R}(\theta_m)$ constructed in section 3. It has to be noted that the numerical cost for solving such a stochastic inverse problem increases with the size N of the random vector $\mathbf{R}$. Consequently, a statistical reducted representation of random vector $\mathbf{R}$

is constructed before solving the stochastic inverse problem. Let $\lambda_1 \geq \ldots \geq \lambda_N$ be the eigenvalues of the covariance matrix $[C_{\mathbf{R}}]$ of random vector $\mathbf{R}$ defined by

$$[C_{\mathbf{R}}] = E\{(\mathbf{R} - \underline{\mathbf{R}})\,(\mathbf{R} - \underline{\mathbf{R}})^T\} \tag{7}$$

in which $\underline{\mathbf{R}} = E\{\mathbf{R}\}$. The normalized eigenvectors associated with the eigenvalues $\lambda_1, \ldots, \lambda_N$ are denoted by $\boldsymbol{\varphi}_1, \ldots, \boldsymbol{\varphi}_N$. We then have

$$[C_{\mathbf{R}}]\,\boldsymbol{\varphi}_k = \lambda_k\,\boldsymbol{\varphi}_k \quad , \tag{8}$$

and

$$\boldsymbol{\varphi}_k^T\,\boldsymbol{\varphi}_\ell = \delta_{kk'} \quad \forall k, k' \leq N \quad . \tag{9}$$

Consequently, the random vector $\mathbf{R}$ can be written as

$$\mathbf{R} = \underline{\mathbf{R}} + \sum_{k=1}^{N} Q_k \sqrt{\lambda_k}\boldsymbol{\varphi}_\ell \quad , \tag{10}$$

in which $Q_1, \ldots, Q_N$ are N real-valued random variables defined by

$$Q_k = \frac{1}{\sqrt{\lambda_k}}\boldsymbol{\varphi}_k^T\,(\mathbf{R} - \underline{\mathbf{R}})\,. \tag{11}$$

From Eqs. (7) - (11) it can be deduced that $Q_1, \ldots, Q_N$ are N real-valued normalized centered random variables such that for all k and ℓ,

$$E\{Q_k\} = 0 \quad , \quad \text{and} \quad E\{Q_k Q_\ell\} = \delta_{k\ell} \quad . \tag{12}$$

Figure 5 displays the graph of the function $n \mapsto \sum_{k=1}^{n} \lambda_k^2$. It can be deduced that random vector $\mathbf{R}$ can be approximated by the random vector $\mathbf{R}^n$ defined by

$$\mathbf{R}^n = \underline{\mathbf{R}} + \sum_{k=1}^{n} Q_k \sqrt{\lambda_k}\boldsymbol{\varphi}_\ell \quad , \tag{13}$$

with $n = 15 < N$. Eqs. (13) can be rewritten as

$$\mathbf{R}^n = \underline{\mathbf{R}} + [\Phi]\,[\Lambda]\mathbf{Q}^n \quad , \tag{14}$$

in which the invertible $(n \times n)$ matrix $[\Lambda]$ and the orthogonal $(N \times n)$ matrix $[\Phi]$ are such that $[\Lambda]_{\ell k} = \delta_{\ell k}\sqrt{\lambda_\ell}$ and $[\Phi]_{\ell k} = [\boldsymbol{\varphi}_k]_\ell$ and where $\mathbf{Q}^n = (Q_1, \ldots, Q_n)$. Futhermore, Eqs. (12) and (14) yields

$$E\{\mathbf{Q}^n\} = 0 \quad , \quad \text{and} \quad E\{\mathbf{Q}^n\,\mathbf{Q}^{n\,T}\} = [I_n]\,, \tag{15}$$

and

$$\mathbf{Q}^n = [\Lambda]^{-1}[\Phi]^T(\mathbf{R} - \underline{\mathbf{R}})\,, \tag{16}$$

in which $[\,I_n]$ is the $(n \times n)$ unit matrix. Let $\mathbf{Q}^n(\theta_1), \ldots, \mathbf{Q}^n(\theta_m)$ be m realizations of random vector $\mathbf{Q}^n$. From Eq. (16) , it is deduced that

$$\mathbf{Q}^n(\theta_j) = [\Lambda]^{-1}[\Phi]^T(\mathbf{R}(\theta_j) - \underline{\mathbf{R}}) \quad , \quad \forall j = 1, \ldots, m$$

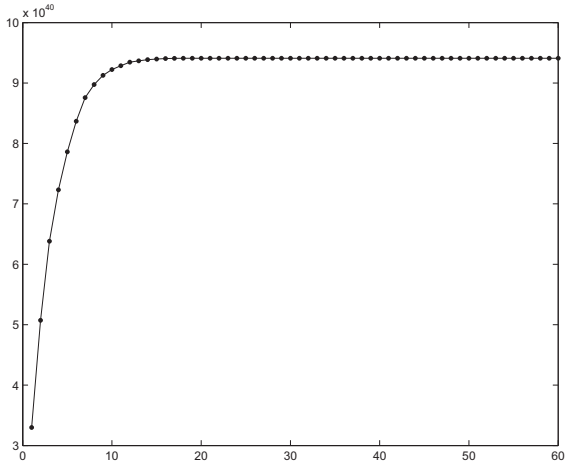

Fig. 5 Convergence analysis of the statistical reduction : graph of function $n \mapsto \sum_{k=1}^{n} \lambda_k^2$. Horizontal axis n, vertical axis $\sum_{k=1}^{n} \lambda_k^2$

5 Polynomial Chaos decomposition

Let $\mathbf{W}^\nu = (W_1, \ldots, W_\nu)$ be the normalized Gaussian random vector such that $E\{W_i W_j\} = \delta_{ij}$. The Chaos representation of the $\mathbb{R}^n$-valued random variable $\mathbf{Q}^n$ in terms of $\mathbf{W}^\nu$ is written as

$$\mathbf{Q}^{n,\nu} = \sum_{\boldsymbol{\alpha},|\boldsymbol{\alpha}|=1}^{+\infty} \mathbf{a}_{\boldsymbol{\alpha}}\,H_{\boldsymbol{\alpha}}(\mathbf{W}^\nu) \quad , \tag{17}$$

where $\boldsymbol{\alpha}$ is a multi-index $(\alpha_1, \ldots, \alpha_\nu)$ belonging to $\mathbb{R}^\nu$, $|\boldsymbol{\alpha}| = \alpha_1 + \ldots + \alpha_\nu$ and where

$$H_{\boldsymbol{\alpha}}(\mathbf{W}^\nu) = H_{\alpha_1}(W_1) \times \ldots \times H_{\alpha_\nu}(W_\nu) \quad ,$$

in which $H_{\alpha_k}(W_k)$ is the normalized Hermite polynomial of order α_k such that

$$\int_{\mathbb{R}} H_{\alpha_k}(w)\,H_{\alpha_j}(w)\frac{1}{\sqrt{2\pi}}e^{-\frac{1}{2}w^2}\,dw = \delta_{\alpha_k\alpha_j}\,.$$

Considering Eqs. (15) , it can be seen that the $\mathbb{R}^n$-valued random variable $\mathbf{Q}^{n,\nu}$ has to be such that

$$E\{\mathbf{Q}^{n,\nu}\,\mathbf{Q}^{n,\nu T}\} = [I_n] \quad , \tag{18}$$

Consequently, the coefficients $\mathbf{a}_{\boldsymbol{\alpha}}$ belonging to $\mathbb{R}^n$ are such that

$$\sum_{\boldsymbol{\alpha},|\boldsymbol{\alpha}|=1}^{+\infty} \mathbf{a}_{\boldsymbol{\alpha}}\mathbf{a}_{\boldsymbol{\alpha}}^T = [\,I_n] \quad . \tag{19}$$

The truncated Chaos representation of random vector $\mathbf{Q}^{n,\nu}$ is denoted as $\mathbf{Q}^{n,\nu,d}$ and is defined by

$$\mathbf{Q}^{n,\nu,d} = \sum_{\boldsymbol{\alpha},|\boldsymbol{\alpha}|=1}^{d} \mathbf{a}_{\boldsymbol{\alpha}}\,H_{\boldsymbol{\alpha}}(\mathbf{W}^\nu) \quad . \tag{20}$$

Substituting $\mathbf{R}$ by $\mathbf{R}^n$ in Eq. (2) and $\mathbf{Q}^n$ by $\mathbf{Q}^{n,\nu,d}$ in Eq. (14) , it can be deduced that, for all $\mathbf{x} \in \mathcal{D}$, the random Young modulus $\widetilde{Y}(\mathbf{x})$ can be approximated by the random variable $\widetilde{Y}^{n,\nu,d}(\mathbf{x})$ defined by

$$\widetilde{Y}^{n,\nu,d}(\mathbf{x}) = \mathbf{h}(x_1)^T \, (\underline{\mathbf{R}} + [\Phi]\,[\Lambda]\mathbf{Q}^{n,\nu,d}) \quad . \tag{21}$$

Obviously, Eq. (21) can be rewritten as

$$\widetilde{Y}^{n,\nu,d}(\mathbf{x}) = \mathbf{h}(x_1)^T \, (\underline{\mathbf{R}} + \sum_{\boldsymbol{\alpha},|\boldsymbol{\alpha}|=1}^{d} [\Phi]\,[\Lambda]\,\mathbf{a}_{\boldsymbol{\alpha}}\, H_{\boldsymbol{\alpha}}(\mathbf{W}^{\nu})) \quad .$$

6 Remark on the identification of the coefficients of the polynomial chaos decomposition by solving a least square optimization problem

The objective of this section is to show that a least square optimization method is not adapted to the available information in order to calculate coefficients $\{\mathbf{a}_{\boldsymbol{\alpha}}, |\boldsymbol{\alpha}| = 1, \ldots, d\}$. Let $\mathbf{Q}^{n,\nu,d}(\theta_1), \ldots, \mathbf{Q}^{n,\nu,d}(\theta_m)$ be m realizations of random variable $\mathbf{Q}^{n,\nu,d}$. We then have,

$$\mathbf{Q}^{n,\nu,d}(\theta_j; \mathbb{A}) = \sum_{\boldsymbol{\alpha},|\boldsymbol{\alpha}|=1}^{d} \mathbf{a}_{\boldsymbol{\alpha}}\, H_{\boldsymbol{\alpha}}(\mathbf{W}^{\nu}(\theta_j)) \ , \ \forall j = 1, \ldots, m$$

in which $\mathbb{A} = \{\mathbf{a}_{\boldsymbol{\alpha}}, |\boldsymbol{\alpha}| = 1, \ldots, d\}$ and where $\mathbf{W}^{\nu}(\theta_1), \ldots, \mathbf{W}^{\nu}(\theta_m)$ are m realizations of the random variable $\mathbf{W}^{\nu}$. A least square method would consist in calculating coefficients $\{\mathbf{a}_{\boldsymbol{\alpha}}, \ |\boldsymbol{\alpha}| = 1, \ldots, d\}$ by solving the least square optimization problem

$$\min_{\mathbb{A}} \Big(\sum_{j=1}^{m} \|\mathbf{Q}^{n,\nu,d}(\theta_j; \mathbb{A}) - \mathbf{Q}^{n}(\theta_j)\|^2\Big) \ , \ \forall j = 1, \ldots, m. \tag{22}$$

Such a method requires that the realizations $\mathbf{W}^{\nu}(\theta_1), \ldots, \mathbf{W}^{\nu}(\theta_m)$ be known for each specimen of the experimental database, that is not the case. Consequently, such a method cannot be used. This is the reason why a method based on the maximum likelihood method is proposed (see [3]).

7 Identification of the coefficients of the polynomial chaos decomposition

7.1 The maximum likelihood method

The maximum likelihood method (see for instance [10]) is used to estimate parameters $\mathbf{a}_{\boldsymbol{\alpha}}$ from realizations $\mathbf{Q}^{n}(\theta_1), \ldots, \mathbf{Q}^{n}(\theta_m)$. We then have to solve the following problem of optizimation: find $\mathbb{A} = \{\mathbf{a}_{\boldsymbol{\alpha}}, |\boldsymbol{\alpha}| = 1, \ldots, d\}$ such that

$$\max_{\mathbb{A}} L(\mathbb{A}) \quad , \quad \text{with} \quad \sum_{\boldsymbol{\alpha},|\boldsymbol{\alpha}|=1}^{d} \mathbf{a}_{\boldsymbol{\alpha}}\, \mathbf{a}_{\boldsymbol{\alpha}}^T = [\, I_n] \tag{23}$$

where

$$L(\mathbb{A}) = p_{\mathbf{Q}^{n,\nu,d}}(\mathbf{Q}^{n}(\theta_1); \mathbb{A}) \times \ldots \times p_{\mathbf{Q}^{n,\nu,d}}(\mathbf{Q}^{n}(\theta_m); \mathbb{A})$$

is the likelihood function associated with realizations $\mathbf{Q}^{n}(\theta_1), \ldots, \mathbf{Q}^{n}(\theta_m)$ and where $p_{\mathbf{Q}^{n,\nu,d}}$ is the probability density function of $\mathbf{Q}^{n,\nu,d}$. It has to be noted that the infinite summation $\sum_{\boldsymbol{\alpha},|\boldsymbol{\alpha}|=1}^{\infty}$ in Eq. (19) has to be substituted by a finite summation $\sum_{\boldsymbol{\alpha},|\boldsymbol{\alpha}|=1}^{d}$. Nevertheless, Eq. (19) is still verified for suffisently high values of chaos order d. However, the optimization problem defined by Eq. (23) yields a very high computational cost induced by the estimation of the joint probability density functions $p_{\mathbf{Q}^{n,\nu,d}}(\mathbf{q}^j, \mathbb{A})$ (even for reasonable values of the length n of random vector $\mathbf{Q}^{n,\nu,d}$). Consequently, it is proposed to substitute the usual likelihood function by a pseudo-likelihood function defined as

$$\widetilde{L}(\mathbb{A}) = \prod_{k=1}^{n} p_{Q_k^{n,\nu,d}}(Q_k(\theta_1); \mathbb{A}) \times \ldots \times \prod_{k=1}^{n} p_{Q_k^{n,\nu,d}}(Q_k(\theta_m); \mathbb{A}) \quad , \tag{24}$$

where $\mathbf{Q}^{n} = (Q_1, \ldots, Q_n)$ and $\mathbf{Q}^{n,\nu,d} = (Q_1^{n,\nu,d}, \ldots, Q_n^{n,\nu,d})$ and where $p_{Q_k^{n,\nu,d}}$ is the probability density function of random variable $Q_k^{n,\nu,d}$. Finally, the following problem of optimization is substituted to the problem defined by Eq. (23) . Find $\mathbb{A} = \{\mathbf{a}_{\boldsymbol{\alpha}}, |\boldsymbol{\alpha}| = 1, \ldots, d\}$ such that

$$\max_{\mathbb{A}} \widetilde{L}(\mathbb{A}) \quad , \quad \text{with} \quad \sum_{\boldsymbol{\alpha},|\boldsymbol{\alpha}|=1}^{d} \mathbf{a}_{\boldsymbol{\alpha}}\, \mathbf{a}_{\boldsymbol{\alpha}}^T = [\, I_n] \quad . \tag{25}$$

7.2 Algorithm for the maximum likelihood optimization

The solver used for constructing the solutions of the optimization problem defined by Eqs. (25) is based on an incremental random search algorithm. This is not the most efficient solver, but it is the simplest one. A key of the method is to substitute coefficients $\mathbb{A}$ by realizations of random coefficients $\{\mathbf{A}_{\boldsymbol{\alpha}}, |\boldsymbol{\alpha}| = 1, \ldots, d\}$ such that

$$\sum_{\boldsymbol{\alpha},|\boldsymbol{\alpha}|=1}^{d} \mathbf{A}_{\boldsymbol{\alpha}}\, \mathbf{A}_{\boldsymbol{\alpha}}^T = [\, I_n] \quad . \tag{26}$$

Let $[\mathbf{A}]$ be a rectangular matrix whose columns are constituted by the random vectors $\{\mathbf{A}_{\boldsymbol{\alpha}}, |\boldsymbol{\alpha}| = 1, \ldots, d\}$. Random matrix $[\mathbf{A}]$ is a $n \times \ell$ matrix where $\ell = \sum_{\boldsymbol{\alpha},|\boldsymbol{\alpha}|=1}^{d} I_{\alpha}$ with $I_{\alpha} = 1$ for all α. From Eq. (26) , it is deduced that

$$[\mathbf{A}]\,[\mathbf{A}_{\boldsymbol{\alpha}}]^T = [\, I_n] \quad . \tag{27}$$

Consequently, realizations of random coefficients $\{\mathbf{A}_{\boldsymbol{\alpha}}, |\boldsymbol{\alpha}| = 1, \ldots, d\}$ can be deduced from realizations of random matrix $[\mathbf{A}]$ satisfying Eq. (27) . Realizations $[\mathbf{A}(\theta)]$ of random matrix $[\mathbf{A}]$ are constructed by using the following algorithm.

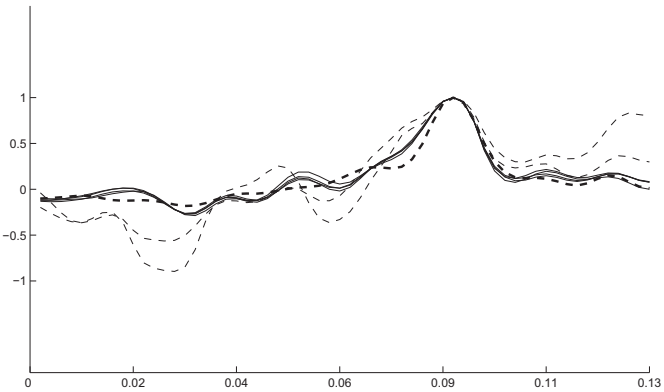

Fig. 6 Graphs of functions $\mathbf{x} \mapsto E\{\mathcal{Y}(\mathbf{x})\mathcal{Y}(\mathbf{x}')\}$ (thick dashed line) and $\mathbf{x} \mapsto E\{\widetilde{\mathcal{Y}}^{n,\nu,d}(\mathbf{x})\widetilde{\mathcal{Y}}^{n,\nu,d}(\mathbf{x}')\}$ where $\mathbf{x} = (x_1, x_2, x_3)$ and $\mathbf{x}' = (x_1', x_2', x_3')$ with $x_1 = 0.0520$, $x_2 = x_3 = 0$ and $x_2' = x_3' = 0$ with $d = 5$, $n = 15$, $\nu = 2, 3$ (thin dashed lines) and $\nu = 4, 5, 6, 7$ (thin solid lines). Horizontal axis: x_1. Vertical axis: $E\{\mathcal{Y}(\mathbf{x})\mathcal{Y}(\mathbf{x}')\}$ and $E\{\widetilde{\mathcal{Y}}^{n,\nu,d}(\mathbf{x})\widetilde{\mathcal{Y}}^{n,\nu,d}(\mathbf{x}')\}$

1. Let $[\mathbf{A}_0]$ be a $n \times \ell$ random matrix whose entries are independent uniform real random variables on $[-1\,, 1]$.
2. Let $[\mathbf{L}]$ be a random upper triangular matrix corresponding to the Chowlesky decomposition of random matrix $[\mathbf{B}_0] = [\mathbf{A}_0][\mathbf{A}_0]^T$. We then have $[\mathbf{B}_0] = [\mathbf{L}]^T[\mathbf{L}]$.
3. It can be proved that Eq. (27) is satisfied by the random matrix $[\mathbf{A}]$ defined as $[\mathbf{A}] = [\mathbf{L}]^{-T}[\mathbf{A}_0]$.We then have $[\mathbf{A}(\theta)] = [\mathbf{L}(\theta)]^{-T}[\mathbf{A}_0(\theta)]$.

7.3 Convergence Analysis

In order to perform a convergence analysis of the method proposed in this paper, the normalized random variables $\mathcal{Y}(\mathbf{x})$ and $\widetilde{\mathcal{Y}}^{n,\nu,d}(\mathbf{x})$ are introduced and defined by

$$\mathcal{Y}(\mathbf{x}) = Y(\mathbf{x})/E\{Y(\mathbf{x})\} \quad , \quad \forall \mathbf{x} \in \mathcal{D}$$

and

$$\widetilde{\mathcal{Y}}^{n,\nu,d}(\mathbf{x}) = \widetilde{Y}^{n,\nu,d}(\mathbf{x})/E\{\widetilde{Y}^{n,\nu,d}(\mathbf{x}) \quad . \quad \forall \mathbf{x} \in \mathcal{D}$$

Figure 6 shows the graphs of functions $\mathbf{x} \mapsto E\{\mathcal{Y}(\mathbf{x})\mathcal{Y}(\mathbf{x}')\}$ (thick dashed line) and $\mathbf{x} \mapsto E\{\widetilde{\mathcal{Y}}^{n,\nu,d}(\mathbf{x})\widetilde{\mathcal{Y}}^{n,\nu,d}(\mathbf{x}')\}$ where $\mathbf{x} = (x_1, x_2, x_3)$ and $\mathbf{x}' = (x_1', x_2', x_3')$ with $x_2 = x_3 = 0$ and $x_2' = x_3' = 0$, for $x_1' = 0.0888$ and with $d = 5$, $n = 15$, $\nu = 2, 3$ (thin dashed lines) and $\nu = 4, 5, 6, 7, 8$ (thin solid lines). It can be seen that the probabilistic model is converged for $\nu = 4$. The remaining error is due to the truncating of the statistical reduction defined in Section 5.

7.4 Identification of the probabilistic model

Each Fig. 7 shows the graphs of $\mathbf{x} \mapsto E\{\mathcal{Y}(\mathbf{x})\mathcal{Y}(\mathbf{x}')\}$ (thick dashed line) and $\mathbf{x} \mapsto E\{\widetilde{\mathcal{Y}}^{n,\nu,d}(\mathbf{x})\widetilde{\mathcal{Y}}^{n,\nu,d}(\mathbf{x}')\}$ (thin solid line) where $\mathbf{x} = (x_1, x_2, x_3)$ and $\mathbf{x}' = (x_1', x_2', x_3')$ with $x_2 = x_3 = 0$ and $x_2' = x_3' = 0$, for $x_1' = 0.0173$ (Fig. 7a), $x_1' = 0.0520$ (Fig. 7b), $x_1' = 0.0888$ (Fig. 7c), $x_1' = 0.1105$ (Fig. 7d) and with $d = 5$, $n = 15$, $\nu = 4$. For all $\mathbf{x} \in \mathcal{D}$, let $y \mapsto p_{\mathcal{Y}(\mathbf{x})}(y;\mathbf{x})$ and $y \mapsto p_{\widetilde{\mathcal{Y}}^{n,\nu,d}(\mathbf{x})}(y;\mathbf{x})$ be the probability density functions of the random variables $\mathcal{Y}(\mathbf{x})$ and $\widetilde{\mathcal{Y}}^{n,\nu,d}(\mathbf{x})$. Each Fig. 8 shows the graphs of $y \mapsto \log_{10}(p_{\mathcal{Y}(\mathbf{x})}(y;\mathbf{x}))$ (thick solid line) and $y \mapsto \log_{10}(p_{\widetilde{\mathcal{Y}}^{n,\nu,d}(\mathbf{x})}(y;\mathbf{x}))$ (thin solid line) where $\mathbf{x} = (x_1, x_2, x_3)$ with $x_2 = x_3 = 0$ and $x_1 = 0.0152$ (Fig. 8a), $x_1 = 0.1018$ (Fig. 8b) and with $d = 5$, $n = 15$ and $\nu = 4$. It can be seen that the probabily density function is accurately identified.

8 Conclusion

A method for solving the stochastic inverse problem using chaos representation of the stochastic field to be identified and an experimental database is proposed. This method extends the method proposed in [3] to the case of experimental vibration tests. The proposed method uses the maximum likelihood principle to identify the coefficients of the chaos representation. For presented example, this method allows any probabilistic quantities to be identified such as the autocorrelation function of the random field and the marginal probability density functions. It should be noted that the proposed method can easily be extended to the case of a viscoelastic random medium for which the elastic properties depend on frequency.

Appendix A. Probabilistic model of the random field modelling the Young modulus of the specimens

The Young modulus of the specimens is modeled by a random field denoted as Y defined by

$$Y(\mathbf{x}) = c_0\, g(c_1, c_2\, V(\mathbf{x})) \quad , \quad \forall \mathbf{x} \in \mathcal{D} \tag{28}$$

in which $c_0 = 1.6663 \times 10^{10}\ N.m^{-2}$, $c_1 = 1.5625$ and $c_2 = 0.2$. The function $\theta \mapsto g(\alpha, \theta)$ from $\mathbb{R}$ into $]0\,, +\infty[$ is such that, for all θ in $\mathbb{R}$,

$$h(\alpha, \theta) = F_{\Gamma_\alpha}^{-1}(F_\Theta(\theta)) \quad ,$$

in which $\theta \mapsto F_\Theta(\theta) = P(\Theta \leq \theta)$ is the cumulative distribution function of the normalized Gaussian random variable Θ and where the function $p \mapsto F_{\Gamma_\alpha}^{-1}(p)$ from $]0\,, 1[$ into $]0\,, +\infty[$ is the reciprocal function of the cumulative distribution function $\gamma \mapsto F_{\Gamma_\alpha}(\gamma) = P(\Gamma_\alpha \leq \gamma))$ of the gamma random variable Γ_α with parameter α. In the right-hand side of Eq. (28) , $\{V(\mathbf{x}), \mathbf{x} \in \mathcal{D}\}$ is a second-order random field such that

$$E\{V(\mathbf{x})\} = 0 \quad \text{and} \quad E\{V(\mathbf{x})^2\} = 1,$$

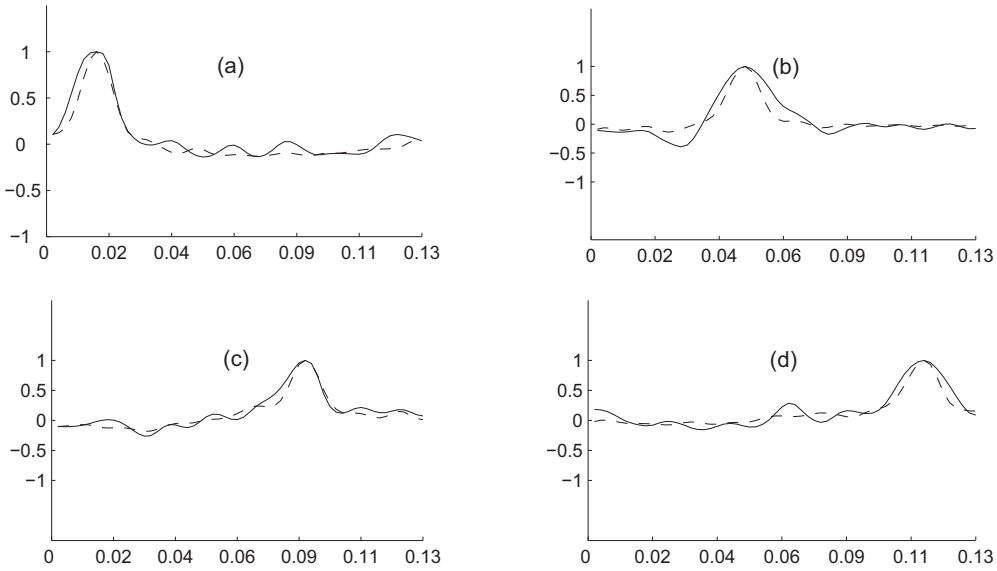

Fig. 7 Graphs of $\mathbf{x} \mapsto E\{\mathcal{Y}(\mathbf{x})\mathcal{Y}(\mathbf{x}')\}$ (thick dashed line) and $\mathbf{x} \mapsto E\{\widetilde{\mathcal{Y}}^{n,\nu,d}(\mathbf{x})\widetilde{\mathcal{Y}}^{n,\nu,d}(\mathbf{x}')\}$ (thin solid line) where $\mathbf{x} = (x_1, x_2, x_3)$ and $\mathbf{x}' = (x_1', x_2', x_3')$ with $x_2 = x_3 = 0$ and $x_2' = x_3' = 0$, for $x_1' = 0.0173$ (Fig. 7a), $x_1' = 0.0520$ (Fig. 7b), $x_1' = 0.0888$ (Fig. 7c), $x_1' = 0.1105$ (Fig. 7d) and with $q = 5$, $n = 15$, $\nu = 4$. Horizontal axis: x_1. Vertical axis: $E\{\mathcal{Y}(\mathbf{x})\mathcal{Y}(\mathbf{x}')\}$ and $E\{\widetilde{\mathcal{Y}}^{n,\nu,d}(\mathbf{x})\widetilde{\mathcal{Y}}^{n,\nu,d}(\mathbf{x}')\}$

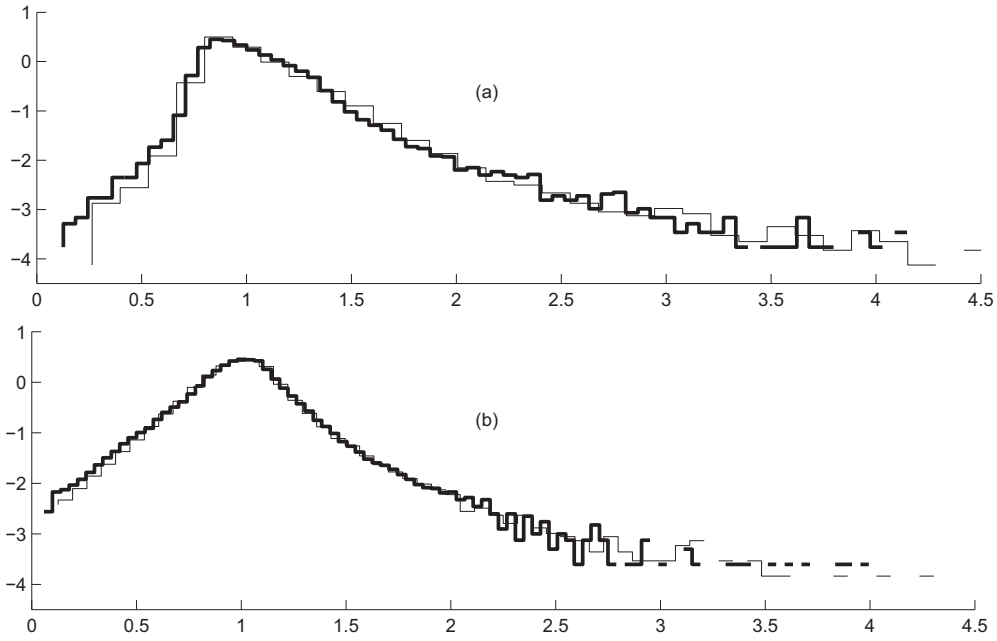

Fig. 8 Graphs of $y \mapsto \log_{10}(p_{\mathcal{Y}(\mathbf{x})}(y;\mathbf{x}))$ (thick solid line) and $y \mapsto \log_{10}(p_{\widetilde{\mathcal{Y}}^{n,\nu,d}(\mathbf{x})}(y;\mathbf{x}))$ (thin solid line) where $\mathbf{x} = (x_1, x_2, x_3)$ with $x_2 = x_3 = 0$ and $x_1 = 0.0152$ (Fig. 8a), $x_1 = 0.1018$ (Fig. 8b) and with $d = 5$, $n = 15$ and $\nu = 4$. Horizontal axis: y. Vertical axis: $\log_{10}(p_{\mathcal{Y}(\mathbf{x})}(y;\mathbf{x}))$ and $\log_{10}(p_{\widetilde{\mathcal{Y}}^{n,\nu,d}(\mathbf{x})}(y;\mathbf{x}))$.

defined by

$$V(\mathbf{x}) = \sum_{|\boldsymbol{\alpha}|=1}^{3} H_{\boldsymbol{\alpha}}(Z_1, Z_2, Z_3, Z_4)\, \sqrt{\gamma_{\boldsymbol{\alpha}}}\, \psi_{\boldsymbol{\alpha}}(\mathbf{x}/2) \quad , \quad (29)$$

in which $\{Z_1, Z_2, Z_3, Z_4\}$ are independent normalized Gaussian random variables, $\boldsymbol{\alpha}$ is a multi-index belonging to $\mathbb{N}^4$ and where $H_{\boldsymbol{\alpha}}(z_1, z_2, z_3, z_4)$ is the multi-indexed Hermite polynomials (see section 5). In the right-hand side of Eq. (29) , $\{\gamma_{\boldsymbol{\alpha}}\}_{1\leq|\boldsymbol{\alpha}|\leq 3}$ and $\{\psi_{\boldsymbol{\alpha}}\}_{1\leq|\boldsymbol{\alpha}|\leq 3}$ are defined as the eigenvalues and the eigenfunctions of the integral linear operator $\mathbf{C}$ defined by the kernel

$$C(\mathbf{x}, \mathbf{x}') = \exp\left(-|x_1 - x_1'|/L\right)$$

in which $L = L_1/40$ and where $\mathbf{x} = (x_1, x_2, x_3)$ and $\mathbf{x}' = (x_1', x_2', x_3')$ belong to $\mathcal{D}$. This means that the correlation length of the random field is much smaller than the length L_1 of the specimen. The eigenvalue problem related to operator $\mathbf{C}$ is then written as

$$\int_{\mathcal{D}} C(\mathbf{x}, \mathbf{x}')\psi_{\boldsymbol{\alpha}}(\mathbf{x}')d\mathbf{x}' = \gamma_{\boldsymbol{\alpha}}\psi_{\boldsymbol{\alpha}}(\mathbf{x}) \quad . \quad (30)$$

It should be noted that, $Y(\mathbf{x}) = Y(x_1)$ and consequently, $Y(\mathbf{x})$ is independent of x_2 and x_3.

Appendix B. Construction of the experimental database by numerical simulation of the direct problem.

In this paper, the experimental database is constructed by numerical simulations of the direct problem. The finite element mesh of the structure is shown in Fig. 1 and consists of 8-node isoparametric 3D solid finite elements. There are $N_d = 1620$ degrees of freedom. Let $\mathbf{Z} = (Z_1, Z_2, Z_3, Z_4)$ be the $\mathbb{R}^4$-valued random variable constituted of the 4 independent random variables in Eq. (29) (the random germ of uncertainties). Let $[K(\mathbf{Z})]$ be the random stiffness matrix with values in the set of all the positive-definite symmetric $(N_d \times N_d)$ real matrices. The $\mathbb{R}^{N_d}$-valued random-frequency-response function $\omega \mapsto \mathbf{U}(\mathbf{Z};\omega)$ related to the nodal displacements is such that

$$[A(\omega;\mathbf{Z})]\mathbf{U}(\mathbf{Z};\omega) = \mathbf{f}(\omega) \quad ,$$

in which

$$[A(\omega;\mathbf{Z})] = \; -\omega^2\,[M] + i\,\omega\,[D] + [K(\mathbf{Z})]$$

where matrices $[M]$ and $[D]$ are defined in section 3 and where $\mathbf{f}(\omega)$ is the $\mathbb{R}^{\mathbb{N}_d}$-vector of the external forces. Let $\mathbf{z}^1, \ldots, \mathbf{z}^m$ be m realizations of random vector $\mathbf{Z}$. The experimental database is then constitued of the m vectors $\mathbf{u}_{\Gamma}^1(\omega), \ldots, \mathbf{u}_{\Gamma}^m(\omega)$ defined as, for all ω in the frequency band of analysis,

$$\mathbf{u}_{\Gamma}^1(\omega) = \mathbb{P}(\mathbf{U}(\mathbf{z}^1;\omega)) \quad , \quad \ldots \quad , \quad \mathbf{u}_{\Gamma}^m(\omega) = \mathbb{P}(\mathbf{U}(\mathbf{z}^m;\omega)) \quad ,$$

where the mapping $\mathbb{P}$ is defined by Eq. (3) .

References

1. Angulo J.M, Ruiz-Medina M.D (1999) Multi-Resolution Approximation to the Stochastic Inverse Problem. Advances in Applied Probability 31(4), 1039–1057.
2. Capilla J.E, Gomez J.J, Sahuquillo A, Franssen H.J.W.M.H (2000) Stochastic Inverse Problems in Groundwater Modeling. Water Studies 7, 295–304.
3. Desceliers C, Ghanem R, Soize C (2004) Maximum Likelihood Estimation of Stochastic Chaos Representations from Experimental Data. (accepted for publication in IJNME)
4. Ghanem R, Spanos P (1991) Stochastic Finite Elements: A Spectral Approach. Springer-Verlag, New York.
5. Manolis G.D., Bagtzoglou A.C. (1992) Numerical comparative study of wave propagation in inhomogeneous and random media. Computational Mechanics 10(6), 397–413
6. Manolis G.D., Shaw R.P. (1996) Boundary integral formulation for 2D and 3D thermal problems exhibiting a linearly varying stochastic conductivity. Computational Mechanics 17(6), 406–417
7. Marquardt D (1963) An Algorithm for Least-squares Estimation of Nonlinear Parameters. SIAM Journal Applied Mathematics 11: 431–44
8. Quintanilla J (1999) Microstructure and properties of random heterogeneous materials: A review of theoretical results. Polymer Engineering and Science 39(3), 559–585
9. Roberts A.P., Garboczi E.J.(2002) Elastic properties of model random three-dimensional open-cell solids. Journal of the Mechanics and Physics of Solids 50(1), 33–55
10. Serfling R.J (1980) Approximation Theorems of Mathematical Statistics. John Wiley & Sons.
11. Shevtsov B.M (1999) Backscattering and Inverse Problem in Random Media. Journal of Mathematical Physics 40(9), 4359–4373.
12. Soize C (2006) Non-Gaussian positive-definite matrix-valued random fields for elliptic stochastic partial differential operators. (In press)
13. Soize C, Ghanem R (2004) Physical Systems with Random Uncertainties: Chaos Representations with Arbitrary Probability Measure. SIAM Journal of Scientific Computing 26(2), 395–410
14. Spanos P, Ghanem R (1989) Stochastic finite element expansion for random media. Journal of Engineering Mechanics 115(5), 1035–1053
15. Wiener N (1938) The Homogeneous Chaos. American Journal of Mathematics 60: 897–936
16. Tleubergenov M.I (2001) An Inverse Problem for Stochastic Differential Systems. Differential Equations 37(5), 751–753.
17. Torquato S (2002) Random Heterogeneous Materials, Microstructure and Macroscopic Properties. Springer-Verlag, New York.